International Journal of Nanomedicine

Dovepress
open access to scientific and medical research

Open Access Full Text Article

ORIGINAL RESEARCH

Nanocarrier-Assisted Delivery of Berberine Promotes Diabetic Alveolar Bone Regeneration by Scavenging ROS and Improving Mitochondrial Dysfunction

Ye Ming[1–3,*], Xinyi He[1–3,*], Zhenxing Zhao[1–3,*], Xuehuan Meng[1–3], Ye Zhu[1–3], Hao Tan[1–3], Guoyin Yang[1–3], Yun Hu[1–3], Leilei Zheng[1–3]

[1]College of Stomatology, Chongqing Medical University, Chongqing, People's Republic of China; [2]Chongqing Key Laboratory of Oral Diseases and Biomedical Sciences, Chongqing, People's Republic of China; [3]Chongqing Municipal Key Laboratory of Oral Biomedical Engineering of Higher Education, Chongqing, People's Republic of China

*These authors contributed equally to this work

Correspondence: Yun Hu; Leilei Zheng, Chongqing Key Laboratory for Oral Diseases and Biomedical Sciences, Chongqing, People's Republic of China, Tel/Fax +86 23 88860151; +86 23 88860161, Email 500188@hospital.cqmu.edu.cn; zhengleileicqmu@hospital.cqmu.edu.cn

Purpose: Oxidative stress and mitochondrial dysfunction are potential contributors to the compromised tissue regeneration capacity of alveolar bone in diabetic patients. Berberine, an active plant alkaloid, exhibits multiple pharmacological effects including antioxidation, blood glucose- and blood lipid-lowering properties. However, it remains uncertain whether berberine can improve impaired osteogenesis in type 2 diabetes mellitus (T2DM), and its poor solubility and oral bioavailability also constrain its applications in bone regeneration. Thus, our study aimed to probe the effects of berberine on bone marrow stem cells (BMSCs) in a diabetic microenvironment, with a greater emphasis on developing a suitable nano-delivery system for berberine and assessing its capability to repair diabetic alveolar bone defects.

Methods: Firstly, BMSCs were exposed to berberine within a high glucose and palmitate (HG+PA) environment. Reactive oxygen species levels, mitochondrial membrane potential, ATP generation, cell apoptosis, and osteogenic potential were subsequently assessed. Next, we explored the regulatory mechanism of autophagy flux in the positive effects of berberine. Furthermore, a nanocarrier based on emulsion electrospinning for sustained local delivery of berberine (Ber@SF/PCL) was established. We assessed its capacity to enhance bone healing in the alveolar bone defect of T2DM rats through micro-computed tomography and histology analysis.

Results: Berberine treatment could inhibit reactive oxygen species overproduction, mitochondrial dysfunction, apoptosis, and improve osteogenesis differentiation by restoring autophagy flux under HG+PA conditions. Notably, Ber@SF/PCL electrospun nanofibrous membrane with excellent physicochemical properties and good biological safety had the potential to promote alveolar bone remodeling in T2DM rats.

Conclusion: Our study shed new lights into the protective role of berberine on BMSCs under T2DM microenvironment. Furthermore, berberine-loaded composite electrospun membrane may serve as a promising approach for regenerating alveolar bone in diabetic patients.

Keywords: berberine, electrospun nanofibrous membrane, diabetes mellitus, alveolar bone remodeling, autophagy flux

Introduction

Alveolar bone defect induced by chronic periodontitis, tumor resection, or trauma is a perennial problem in clinical practice, which has a serious impact on people's work and life.[1,2] One of the most common causes for alveolar bone loss is periodontitis, and over 1.0 billion people worldwide living with severe periodontal disease, thus leading to irreversible

Received: 2 May 2024
Accepted: 15 September 2024
Published: 9 October 2024

loosening and loss of teeth.[3] Regeneration of alveolar bone defect has always been challenging, which could be exacerbated by systemic diseases such as autoimmune diseases, congenital bone dysplasia, cardiovascular disease, and diabetes mellitus (DM).[4,5] DM is a highly prevalent metabolic disorder, and it is estimated that the number of DM patients will go up to more than 1.31 billion around the world by 2050.[6–8] The abnormal bone turnover and compromised bone remodeling observed in type 2 DM (T2DM) have been ascribed to the overproduction of reactive oxygen species (ROS) in a hyperglycemic microenvironment.[9,10] The mitochondria, as a dominant source of ROS, are often the primary target of excessive ROS attack.[11] Mitochondria dysfunction not only inhibits the production of adenosine triphosphate (ATP) but also exacerbates cellular oxidative stress,[12] which eventually leads to dysfunction, apoptosis, and dedifferentiation of bone-forming cells.[13,14] Furthermore, chronic overload of free fatty acids in T2DM patients can increase the production of ROS, causing synergistic glucolipotoxicity in conjunction with high glucose levels.[15,16] Therefore, a potential strategy for promoting bone regeneration involves eliminating ROS and improving mitochondrial dysfunction resulting from hyperglycemia and hyperlipidemia.

Autophagy is an evolutionarily conserved process that selectively degrades excess misfolded proteins and damaged intracellular components to maintain cellular homeostasis.[17] Abnormal autophagy would exacerbate the accumulation of dysfunctional mitochondria, as well as subsequent bioenergetic deficiencies and oxidative damage.[18] Lytrivi et al identified that impaired autophagy was a key molecular mechanism underlying glucolipotoxic β-cell dysfunction.[16] Based on these findings, we hypothesized that activating autophagy could be a potential solution for eliminating ROS and stabilizing mitochondrial function in T2DM.

Berberine is an active plant alkaloid extracted from rhizoma coptidis, a traditional Chinese medicine.[19] It is known for its various pharmacological effects including blood glucose-lowering, blood lipid-lowering, and antioxidant properties.[20–23] It was reported that berberine could alleviate cell injury by scavenging ROS and improving mitochondrial dysfunction in previous studies.[24,25] In addition, increasing evidence demonstrated that berberine was able to ameliorate cell apoptosis by up-regulation of autophagy.[21,26,27] Li et al observed that berberine could protect D407 cells against H_2O_2-induced cytotoxicity through activating autophagy-mediated ROS elimination.[26] Given these studies, berberine might be able to improve unfavorable diabetic micromilieu and boost alveolar bone formation. However, the poor solubility and oral bioavailability of berberine limit its applications in DM, although berberine has a broad range of sources and not expensive. Therefore, there is an urgent need to develop a suitable delivery system to enhance its bioavailability for diabetic bone tissue repair.

Among various local delivery systems, electrospinning is a promising technique that can encapsulate drugs, proteins, and growth factors in polymeric nanofibers by a simplistic and cost-effective method.[28–30] Moreover, electrospun mats can mimic bone extracellular matrix (ECM) structure and provide enough space for cell adhesion and proliferation due to their high porosity and pore interconnectivity.[31] Silk fibroin (SF), a versatile biopolymer produced by silkworm, has been identified as a potential drug carrier due to its excellent properties such as non-cytotoxicity, tailorable biodegradability, low immunogenicity, and the ability to maintain drug stability.[32–34] But the poor mechanical performance of pure SF nanofibrous membranes limits their applications as structural materials.[35] This can be addressed by blending SF with polycaprolactone (PCL), a synthetic polymer known for its mechanical strength.[36] However, an unexpected burst of drug release was commonly observed in the SF/PCL composite nanofibers prepared by blending electrospinning.[37] Fortunately, this can be overcome by constructing core-shell nanofibers via emulsion electrospinning. Such nanofibers can embed small-molecule drugs in the core layer and release them in a sustained and controlled manner.[38]

Herein, we found that berberine promoted autophagy in bone marrow stem cells (BMSCs) under diabetic microenvironment. This helped to reduce ROS and improve mitochondrial dysfunction, ultimately rescuing the impaired BMSCs. Notably, we synthesized a core-shell electrospun nanofibrous membrane (Ber@SF/PCL) via emulsion electrospinning. This membrane allowed for a local and persistent release of berberine by encapsulating it in the core layer. We then evaluated the physicochemical characterization, biocompatibility, and efficacy of the nanofiber mats in repairing alveolar bone defects in T2DM rats. It is believed that our study offers a new therapeutic option for regenerating diabetic alveolar bone (Figure 1).

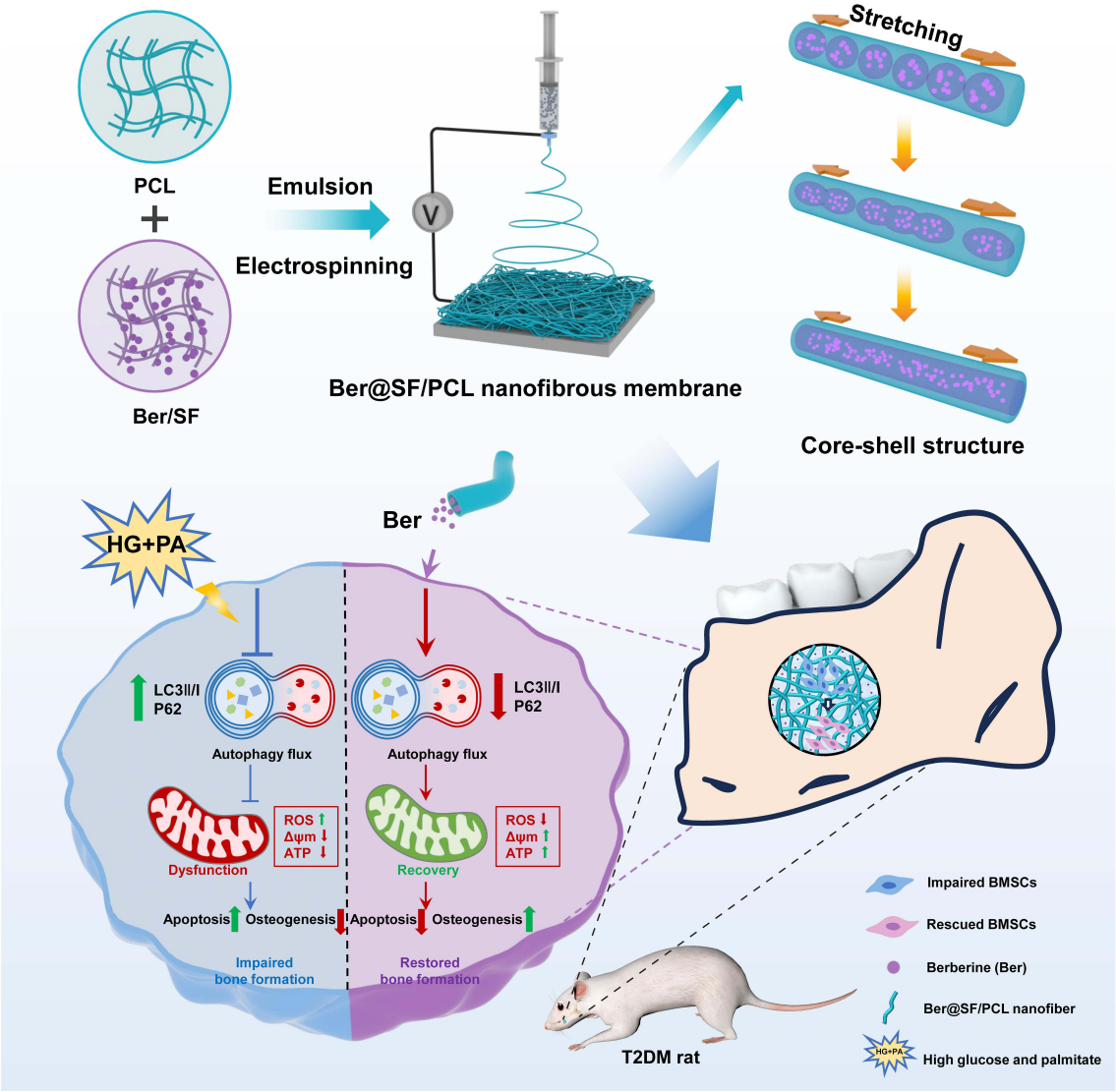

Figure 1 Schematic diagram depicting how berberine rescued the impaired BMSCs through the restoration of autophagy flux under HG+PA conditions as well as the design principle of berberine-loaded core-sheath nanofibrous membrane (Ber@SF/PCL) based on emulsion electrospinning for diabetic alveolar bone regeneration.

Materials and Methods

Cell Culture

BMSCs were harvested from Sprague Dawley rats (4 weeks, ♂), as reported in our previous study.[39] Simply, cells were cultivated in complete medium including double antibiotics (Hyclone, Logan, Utah, USA, SV30010) (1%), fetal bovine serum (Lonsera, Suzhou, China, S711-001S) (10%) and α-Minimum Essential Medium (Hyclone, Logan, Utah, USA, SH30265.01) (89%) in a humidified incubator (5% CO_2, 37°C) (Thermo Fisher, Massachusetts, USA). After trypsinization, BMSCs of passage three to five were seeded in plates for the present study. For in vitro experiments, BMSCs were exposed to high glucose (25.5 mM, Sigma, St. Louis, USA, 47249) and palmitate (150 μM, Sigma, St. Louis, USA, P5585) (HG+PA) to mimic the T2DM microenvironment[40,41] for 12 hours or pretreated with berberine (1 μM, Solarbio, Beijing, China, IB0440) for 12 hours.

Intracellular ROS Measurement

The DCFH-DA fluorescent probe (Beyotime, Shanghai, China, S0033S) was selected to measure the level of intracellular ROS. Briefly, BMSCs were incubated in fresh serum-free medium containing this fluorescent probe (10 μM) for

30 minutes at 37°C, while being protected from light. After the incubation period, we removed the medium, rinsed the cells with phosphate buffered saline (PBS, Boster, Wuhan, China, PYG0021) thrice, and observed the green fluorescence signals through a fluorescence microscope (Nikon, Tokyo, Japan), which were quantified by the ImageJ software.

Detection of Mitochondrial Membrane Potential (MMP)

The MMP change in BMSCs was examined via JC-1 probe (Beyotime, Shanghai, China, C2003S). Following treatment, BMSCs were cultured in complete medium containing JC-1 working solution (2 μM) and incubated for 20 minutes at 37°C. After being washed with JC-1 buffer (1x) twice, the samples were imaged by a fluorescence microscope. Additionally, the ratios between green and red fluorescence were used to determine MMP changes using ImageJ software.

Measurement of ATP Content

The enhanced ATP Assay Kit (Beyotime, Shanghai, China, S0027) was used to measure the intracellular ATP levels of the cells. Cell lysates were prepared with ATP Lysis Buffer, then centrifuged (12,000 rcf, 4°C, 5 min). The supernatant was collected for the next step. Next, 100 μL of ATP prepared working solutions were transferred to black 96-well plates and left at room temperature (RT) for 3 minutes. Afterwards, 20 μL of the supernatants or standards were added to the plates and mixed quickly before the readings were taken using a luminometer in a multifunctional microplate reader (Thermo Fisher, Massachusetts, USA). The final ATP content was calculated based on the standard curve and the total protein concentration.

Flow Cytometry (Apoptotic Experiment)

The apoptosis rate of BMSCs was analyzed using flow cytometry after Annexin-V FITC staining, following the instructions provided in the kit (Beyotime, Shanghai, China, C1062S). Firstly, treated BMSCs were digested at RT and collected in Eppendorf tubes (at least 10^6 cells/tube). After two washes with cold PBS, the BMSCs were resuspended in 1× binding buffer (500 μL). Subsequently, propidium iodide (PI) (5 μL) and Annexin V-FITC (10 μL) were used to stain the cells in each group. The cells were protected from light and incubated at RT for 20 minutes. Finally, the cell suspensions were analyzed using the CytoFlex flow cytometer (Beckman Coulter, California, USA).

Western Blot (WB) Analysis

Cells were lysed with RIPA lysis buffer (Beyotime, Shanghai, China, P0013B) including phenylmethanesulfonyl fluoride (1 mM, Beyotime, Shanghai, China, ST507). After centrifugation (4°C, 14,000 rcf, 5 min), the supernatants were collected. A BCA kit (Beyotime, Shanghai, China, P0010) was adopted to measure protein concentrations in supernatants, which were mixed with 5× loading buffer (Epizyme, Shanghai, China, LT101L) before 100°C degeneration. Equivalent amounts of protein extracts in each group were electrophoretically fractionated by an SDS-polyacrylamide gel (12.5%, Epizyme, Shanghai, China, PG213) and transferred to a polyvinylidene fluoride membrane (0.22 μm pore size, Millipore, Massachusetts, USA). The membrane was sealed with 5% bovine serum albumin (biofroxx, Berlin, Germany, 4240GR005) for 2 hours at RT, and subsequently incubated with the primary antibody for 12–18 hours at 4°C and the secondary antibody at RT for another 2 hours. The membrane was then exposed to ECL developing solution (Epizyme, Shanghai, China, SQ202) and scanned by a ChemiDoc imager (Bio-Rad, Hercules, CA, USA) to visualize the protein band. Finally, the target protein expression was obtained according to the gray value measured by ImageJ software and normalizing to β-actin. The primary and secondary antibodies above were as follows: β-actin (1:5000, Bioss, Beijing, China, bs-0061R), cleaved caspase-9/procaspase-9 (1:1000, 9508), cleaved caspase-3 (1:1000, 9664), LC3-II/I (1:1000, 12741), P62 (1:1000, 23214) (Cell Signaling Technology, Massachusetts, USA), Goat Anti-Rabbit IgG (1:5000, Bioss, Beijing, China, bs-40295G-HRP) and Goat Anti-Mouse IgG (1:5000, Abcam, Cambridge, UK, ab205719).

Alkaline Phosphatase (ALP) Staining

For osteogenic induction, cells were cultured in a complete medium containing ascorbate (5 μM, Solarbio, Beijing, China, A8100), β-glycerophosphate (10 mM, Solarbio, Beijing, China, G8100) and dexamethasone (100 nM, Solarbio,

Beijing, China, D8040). We changed the medium every 2–3 days. After one week, 4% paraformaldehyde (PFA, Biosharp, Anhui, China, MBX113) was used to fix the BMSCs, which were then stained by a BCIP/NBT ALP kit (Beyotime, Shanghai, China, C3206). The results were recorded by scanners, and the microstructure was further observed using a light microscope (Nikon, Tokyo, Japan). The ImageJ software was utilized to quantify the ALP staining.

Quantitative Real Time-Polymerase Chain Reaction (qRT–PCR)

After seven days of osteogenic induction, the TRIzol reagent (Takara, Tokyo, Japan, 9108) was used for harvest total RNA in BMSCs. The cDNA was then acquired using 5× PrimeScript RT Master Mix (Takara, Tokyo, Japan, RR036A). The reaction solutions (10 μL/well) containing cDNA, TB Green Premix Ex Taq (Takara, Tokyo, Japan, RR820A), forward and reverse primers and RNase-free water were mixed for qRT-PCR, which was performed on the Bio-Rad Applied Biosystems ABI 7500 System (Bio-Rad, Hercules, CA, USA). The internal control (*β-actin*) was used to determine the expressions of the osteogenic genes (*Alp, Runx2*). The expression of target gene was analyzed via the ΔΔCt method. The study's primer sequences (Sangon, Shanghai, China) were provided in Table S1.

Transmission Electron Microscope (TEM)

The ultrastructure of autophagosomes and autolysosomes was visualized using TEM (JEOL Ltd., Tokyo, Japan). BMSCs in each group were treated, digested, centrifuged and carefully fixed with a 2% glutaraldehyde fixative solution (Beyotime, Shanghai, China, G916054) for 24 hours at 4°C. The cells then underwent fixation in 1% osmium tetroxide for 60 minutes at 4°C. The samples were subsequently dehydrated, embedded in Epon 816 (Electron Microscopy Sciences, Hatfield, PA, USA), and sliced by a ultramicrotome (Leica Microsystems, Buffalo Grove, IL, USA). Following staining with uranyl acetate and lead citrate, the slides were imaged using TEM.

Preparation of SF

We extracted SF from the cocoons of Bombyx mori silkworms (Beibei Silkworm Egg Co., Chongqing, China) following the method previously reported.[42] Briefly, small pieces of cocoons were degummed using a 0.02 M Na_2CO_3 solution (Aladdin, Shanghai, China, S111733) for 60 minutes at 100°C. The degummed cocoons were then washed with ddH_2O in triplicates and dried at 37°C. Subsequently, the SF fibers were completely dissolved in a LiBr solution (9.3 M, Macklin, Shanghai, China, L812430) in an oven for 4 hours at 65°C. The SF solution was then dialyzed (dialysis bag, MWCO 3500 Da, Solarbio, Beijing, China) against ddH_2O at 4°C for 72 hours, which was changed every 12 hours. After two rounds of centrifugation (4000 rpm, 4°C, 30 min), the supernatant was obtained and lyophilized (Tian Feng, Shanghai, China) for two days to obtain solid, regenerated SF.

Synthesis of Ber@SF/PCL Electrospinning Nanofibrous Membrane

The electrospinning solutions was prepared as previously described with several changes.[43] The PCL (10% w/v, Macklin, Shanghai, China, P871874) was dissolved in a mixture of dichloromethane/hexafluoroisopropanol (DCM/HFIP, Macklin, Shanghai, China, D807825/H811026) (3:1, v/v) and the SF (10% w/v) was dissolved in HFIP. These solutions were stirred at 300 rpm overnight at RT. Berberine was accurately weighed and mixed with the SF/HFIP solution to create different mixtures with concentrations of 0%, 1.25%, 2.5% and 5% (w/w). Next, the PCL/DCM/HFIP solution was added to an equal volume of Ber/SF/HFIP with continuous agitation overnight at RT to form the stable emulsions. The emulsions were then used to fabricate the SF/PCL or Ber@SF/PCL nanofibers via electrospinning using the electrospinning instrument (Yongkang Leye Technology Development Co. Ltd., Beijing, China) with the following process parameters: RT, 45±5% relative humidity, a voltage of 14 kV, a 21-gauge stainless needle, a 5 mL plastic syringe, a distance of 15 cm between the collector and needle, and a constant flow rate of 0.3 mL/h. The collected electrospun membranes were further placed in a ventilated oven for 24 hours to volatilize any remaining solvent. Then, the β-sheet formation of SF was induced by soaking the electrospun mats in methanol (99.5%, Chuandong Chemical Co., Chongqing, China, H1247) for 30 minutes. Finally, the membranes were washed thrice, lyophilized, and stored at RT for the following experiments.

Physical and Chemical Characterization

Scanning electron microscopy (SEM, Thermo Fisher, Massachusetts, USA) at 20 kV was utilized to examine the surface morphology of electrospun nanofibers. The diameter distribution of the nanofibers was measured by ImageJ. A copper grid was used to collect a few nanofibers, and the inner structure of these fibers were visualized using TEM (Hitachi, Tokyo, Japan) at 120 kV. The drug distribution in nanofibers, which contain berberine that exhibits spontaneous fluorescence, was visualized via confocal laser scanning microscopy (Leica, Wetzlar, Germany). Fourier transform infrared spectroscopy (FTIR, Thermo Fisher, Massachusetts, USA) analysis was conducted to investigate the chemical composition of pure berberine, SF/PCL, and Ber@SF/PCL. The analysis was performed in the range of 500–4000 cm^{-1} with a resolution of 2 cm^{-1}. The crystalline phases of the samples were evaluated by an X-ray diffractometer (XRD, Bruker, Karlsruhe, Germany), operated at 300 mA and 40 kV in the range of $5° \leq 2\theta \leq 90°$ with a scan rate of 5° (2θ) min^{-1}. The wettability of the sample surfaces was assessed by the water contact angle (WCA). Briefly, after the drop deposition on the surface of each sample from different groups for 15 seconds, the WCA values were immediately measured using a WCA meter (Huanqiuhengda Technology Co, Beijing, China). The Ber@SF/PCL membrane (10 mg) was immersed in 1.0 mL of PBS (pH=7.4) and placed in a thermostatic oscillator (70 rpm, 37°C). At predetermined time points, 0.7 mL of the supernatant was collected and an equal amount of fresh PBS was added to the tube. The absorbance at 335 nm of the collected supernatant was analyzed using a UV spectrophotometer (Thermo Fisher, Massachusetts, USA). Additionally, the in vitro degradation rate of the nanofibrous membranes was determined by measuring the weight loss over time. 10 mg of the membranes were submerged in PBS containing 300 μg/mL of protease XIV (Sigma, St. Louis, USA, P5147) and incubated in a shaking incubator for 28 days with a rotation speed of 120 rpm at 37°C. The mats were taken out at each time point, washed with ddH_2O, lyophilized, and weighed using an electronic analytical balance (Mettler Toledo, Schwarzenbach, Switzerland). Finally, the calculation formula of the degradation rate was as follows:

$$\text{Degradation rate} = (\text{initial weight} - \text{lyophilized weight})/\text{initial weight} \times 100\%$$

Biocompatibility Evaluation

Cell counting kit-8 (CCK-8, Beyotime, Shanghai, China, C0038) assays and live/dead cell staining were used to evaluate the cell cytotoxicity of the membranes. First, the nanofibrous membranes were UV sterilized for 2 hours on each side. Then, the conditioned medium was prepared by incubating four groups of membranes (0%, 1.25%, 2.5%, 5%) in complete medium for 72 hours at 37°C. BMSCs (1000 cells/well) were plated in 96-well plates and exposed to different conditioned medium. After 1, 4, and 7 days, the medium was changed to 110 μL CCK8 solution (100 μL fresh medium: 10 μL CCK8), and the BMSCs were incubated at 37°C for 2.5 hours away from light. The optical density (OD) value was read at 450 nm using a microplate reader (Thermo Fisher, Massachusetts, USA). Cytotoxicity is calculated as follows:

$$\text{Cytotoxicity} = \left(OD_{\text{condition medium group}} - OD_{\text{blank group}}\right)/\left(OD_{\text{complete medium group}} - OD_{\text{blank group}}\right) \times 100\%.$$

Additionally, BMSCs were plated in 48-well plates at a density of 2000 cells/well and cocultured with or without the conditioned media for 1, 4, and 7 days. After incubation, live and dead cells were treated with the Calcein-AM/PI double staining kit (BestBio, Shanghai, China, BB-4126) and visualized using a fluorescence microscope. Hemolysis analysis was performed to test the biocompatibility of SF/PCL and Ber@SF/PCL membranes. Rat erythrocytes were harvested by centrifuging fresh rat blood at 1000 rpm for 15 minutes, then rinsed three times with saline, and 2% erythrocyte suspension in saline was prepared for the next experiment. The erythrocyte suspension was incubated with the SF/PCL membrane, Ber@SF/PCL membrane, ddH_2O containing Triton X-100 (0.1%, positive control, T8200), and saline (0.9%, negative control) at 37°C. After incubating for 2 hours at RT, samples were photographed and centrifuged for 5 minutes at 1000 rpm. The resultant supernatants were transferred to a 96-well plate, which was read at OD_{570nm} using a microplate reader. The hemolysis percent is calculated as follows:

$$\text{The hemolysis} = \left(OD_{\text{sample}} - OD_{\text{negative}}\right)/\left(OD_{\text{positive}} - OD_{\text{negative}}\right) \times 100\%.$$

To detect the in vivo biotoxicity of the electrospun nanofibrous membranes, the heart, liver, spleen, lung and kidney tissues harvested from T2DM rats were fixed with 4% PFA for hematoxylin and eosin (H&E, Solarbio, Beijing, China, G1120) staining after 6 weeks of membrane implantation.

Animal Experiment

All animal experiments were approved by the ethics committee of the College of Stomatology, Chongqing Medical University (permit number: CQHS-REC-2022 (LSNo.152)) and adhered to the NIH "Guide for the Care and Use of Laboratory Animals". 4-week-old male Sprague-Dawley rats were obtained from the Laboratory Animal Centre of Chongqing Medical University. All rats were housed under a specific-pathogen-free environment with 12-hour light/dark cycles (lights on at 7:30 AM) and a controlled temperature (24 ± 2°C). After acclimation for seven days, all rats were randomized into 4 groups: control group, T2DM group, T2DM+SF/PCL group, and T2DM+Ber@SF/PCL group. After being fed a high-fat diet (Synergy Bio., Jiangsu, China, XTHF45-1) for 4 weeks, the rats were fasted overnight and administrated streptozotocin (STZ, 40 mg/kg, Sigma, St. Louis, USA, S0130) by intraperitoneal injection to induce T2DM, as previously described.[44,45] Age-matched rats of the control group were given a regular diet and treated with equal volumes of citrate buffer (pH=4.5, Solarbio, Beijing, China, C1013) as those in the T2DM groups. T2DM rats were considered successfully inducted if their random non-fasted blood glucose levels were more than 16.7 mmol/L, along with exhibiting polyuria, polydipsia, and weight loss at 7 and 14 days after STZ injection.

Mandibular alveolar bone defects were prepared following the procedure mentioned in literature.[46] Simply, the rats were anesthetized by inhaling isoflurane via an anesthesia machine (Raymain, Shanghai, China), and the skin of the operation area was shaved and strictly sterilized with iodophor. After a 1.0-cm incision was made along the mouth corner, the masseters were separated. The buccal plate was then exposed and a standard round defect (diameter: 3 mm; depth:1 mm) was created at the periapical region between the first and second molars. The sterilized SF/PCL or Ber@SF/PCL electrospun membranes were carefully implanted into the bone defects. At 2 or 6 weeks after the surgery, the rats were euthanized for sample collection. After fixed with 4% PFA for 48 hours, the samples were flushed with tap water overnight and then stored in 70% ethanol at 4°C.

Micro-Computerized Tomography (Micro-CT) Scanning

The scans of specimens were performed using a micro-CT (vivaCT80, SCANCO Medical AG, Basserdorf, Switzerland) at 113 μA, 70 kVp, and 12.5 μm resolution. After three-dimensional (3D) reconstruction of the mandibles, we selected the region of interest and conducted quantitative analysis of alveolar bone changes. The analysis included measuring bone volume/tissue volume (BV/TV), trabecular thickness (Tb.Th), trabecular space (Tb.Sp) and trabecular number (Tb.N).

Histological Analysis

Following μ-CT scanning, the fixed tissues were decalcified in a 20% solution of disodium ethylenediamine tetraacetate (pH 7.4, Sigma, St. Louis, USA, V900081) for 6 weeks. The samples were then dehydrated, embedded with paraffin, and sliced at 5 μm for H&E and Masson's trichrome staining (Solarbio, Beijing, China, G1340). For immunohistochemistry staining (Bioss, Beijing, China, SP-0023), the slides were cultured overnight with the primary antibodies (Runx2 (1:100, bs-1134R), OCN (1:100, bs-0470R)) (Bioss, Beijing, China) at 4°C. After overnight incubation, the primary antibodies were washed off, and the slides were incubated with the secondary antibody for 20 minutes at 37°C. Diaminobenzidine chromogen and hematoxylin counterstaining were then applied. The stained slides were scanned using the SlideView VS200 (Olympus, Tokyo, Japan).

Statistical Analysis

GraphPad Prism 9.0 (San Diego, CA, USA) was utilized to perform all data analysis. Experimental data were presented as mean ± standard deviation from the experiments in triplicate. For comparisons among three or more groups, one-way ANOVA was performed, and the Tukey's test was for multiple comparisons. $p < 0.05$ was indicated statistically significant.

Results and Discussion

Berberine Inhibited ROS Overproduction, Mitochondrial Dysfunction, Cell Apoptosis and Improved Osteogenesis Differentiation Induced by HG+PA in BMSCs

BMSCs are the main sources of osteoblasts, and their functional deficits have been found to remarkably affect the efficiency of bone regeneration during the healing process.[47] The microenvironment of T2DM, usually characterized by

hyperglycemia and hyperlipidemia, can drastically disrupt the biological functions of BMSCs. Understanding the underlying mechanisms of cell behavior in this pathological context is essential for finding an effective therapy for diabetic bone remodeling. Oxidative stress and mitochondrial dysfunction were previously confirmed to perturb bone homeostasis and regeneration under diabetic conditions.[48] Recently, berberine has gained attention for its antioxidant and anti-apoptotic properties.[20] In our study, BMSCs were cultured in the HG+PA environment that mimicked the T2DM milieu to investigate the efficacy of berberine. The fluorescent probe DCFH-DA was applied in detecting intracellular ROS levels: HG+PA treatment led to a significant increase in the green fluorescence intensity, which could be inhibited by berberine (Figure 2A and B). Additionally, we assessed mitochondrial function under HG+PA conditions, focusing on MMP and ATP production level in BMSCs. Berberine treatment mitigated the changes in MMP induced by HG+PA, as shown by the increased ratio of red to green fluorescence from JC-1 staining (Figure 2C and D). Furthermore, HG+PA treatment significantly decreased ATP levels in BMSCs, which was partially reversed by berberine treatment (Figure 2E). The results above demonstrated that berberine could alleviate ROS overproduction and mitochondrial dysfunction in HG +PA-compromised BMSCs.

It is well established that when MMP collapses and mitochondrial membrane permeability increases, pro-apoptotic factors are released from mitochondria into the cytoplasm, triggering the caspase apoptotic cascade; within this cascade, procaspase-9 is recruited and activated, thereby activating executioner caspase-3 and leading to apoptosis.[49] We observed that the level of cell apoptosis and death in HG+PA group was significantly higher than that in control group, while HG +PA+Ber group showed a reduced rate of cell apoptosis and death compared to HG+PA group (Figure 2F and G). We also assessed mitochondrial apoptotic pathway-related proteins (cleaved caspase-3, cleaved caspase-9/ procaspase-9) in BMSCs using WB analysis. As expected, HG+PA treatment increased the levels of cleaved caspase-3 and cleaved caspase-9/procaspase-9, which were significantly reduced by berberine treatment (Figure 2H and I). These results bore similarities with a previous study that demonstrated the ability of berberine to alleviate doxorubicin-induced mitochondrial damage and oxidative injury, thereby preventing apoptosis in cardiac myocytes.[25]

In addition to its role in cell survival, mitochondria play a crucial role as regulators in osteogenic differentiation process.[13,14] When there is persistent mitochondrial dysfunction, the osteogenesis of BMSCs is significant hindered as the requirement for large amounts of energy in this process cannot be fulfilled.[50] In this study, after osteogenic induction for 7 days, HG+PA-induced BMSCs exhibited impaired osteogenic differentiation capacity. This was justified by the decreased ALP staining (Figure 2J and K) and expressions of osteogenic-specific genes including *Runx2 and Alp* (Figure 2L). However, after BMSCs were pretreated with berberine, the impaired osteogenic differentiation potential was markedly improved, as evidenced by the increased ALP staining and expression of osteogenic genes (Figure 2J–L). The findings were quite comparable to previous studies.[51,52] Overall, these results demonstrated that berberine effectively mitigated ROS overproduction, mitochondrial dysfunction, cell apoptosis, and improved osteogenic differentiation under HG+PA conditions. However, the molecular mechanisms underlying the protective effects of berberine needed further investigation.

Berberine Protected BMSCs from Damage Induced by HG+PA via Facilitating Autophagy Flux

Autophagy is a highly conserved catabolic process that clears dysfunctional organelles and abnormal protein aggregates to maintain cell homeostasis.[53] This process is crucial for the survival and differentiation of bone-forming cells like BMSCs.[54] To investigate the impact of HG+PA and berberine on autophagy flux in BMSCs, we measured the expression levels of autophagy-related proteins using WB. The results showed an increase in LC3-II/I and P62, indicating autophagy deficiency under HG+PA conditions. However, the treatment with berberine reversed these changes (Figure 3A). Additionally, TEM revealed that an accumulation of autophagosomes was observed in BMSCs following HG+PA treatment, while berberine reduced the number of autophagosomes and increased that of autolysosomes to upregulate autophagy flux (Figure 3B).

The roles of autophagy in different pathological processes are controversial, and can be either pro-survival or pro-death.[55] To investigate the underlying role of autophagy flux in the protective effects of berberine, BMSCs were pre-treated with the autophagy inhibitor chloroquine (CQ). As expected, CQ pretreatment resulted in the blockage of

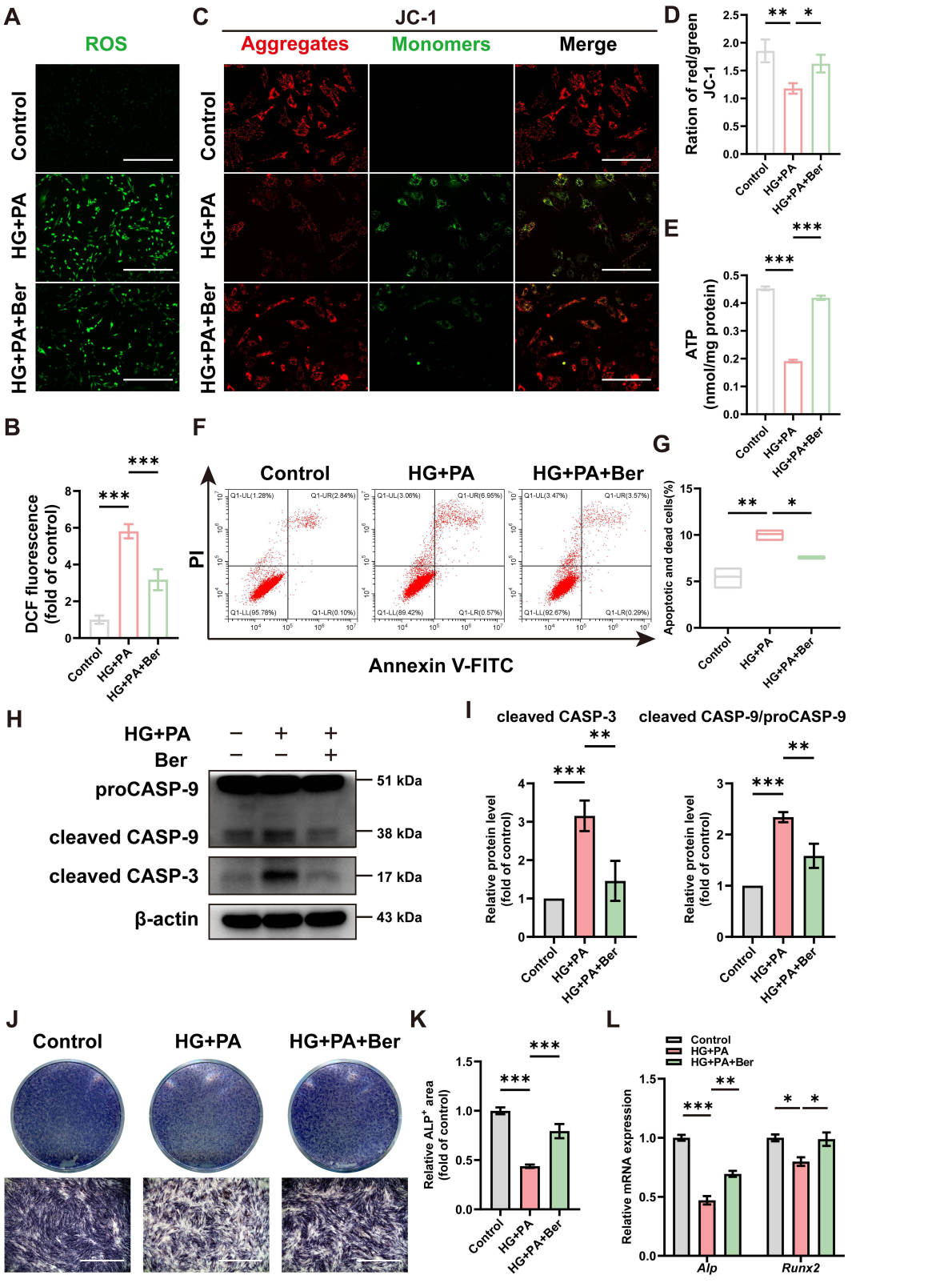

Figure 2 Berberine inhibited ROS overproduction, mitochondrial dysfunction, BMSCs apoptosis and improved osteogenesis differentiation under HG+PA conditions. (**A**) Representative fluorescence images and (**B**) statistical graph of ROS levels in BMSCs from the control, HG+PA, and HG+PA+Ber groups. Scale bar: 400 μm. (**C**) Fluorescence staining images of MMP and (**D**) the ratio of red/green fluorescence signals. Green signal indicated monomeric JC-1, and red signal indicated aggregated JC-1. Scale bar: 200 μm. (**E**) ATP production level in BMSCs. (**F**) Flow cytometry and (**G**) quantitative analysis of the apoptotic and death cells after Annexin-V/PI double staining. (**H**) WB and (**I**) quantitative analysis of cleaved caspase-3 and cleaved caspase-9/procaspase-9 as treated above. (**J**) Typical digital photos and (**K**) quantification analysis of ALP staining on day 7. Scale bar: 1 mm. (**L**) qRT–PCR of the relative gene expressions encoding osteogenic markers *Runx2* and *Alp* in BMSCs. *p < 0.05, **p < 0.01, ***p < 0.001. HG+PA, high glucose and palmitate; Ber, berberine; CASP, caspase.

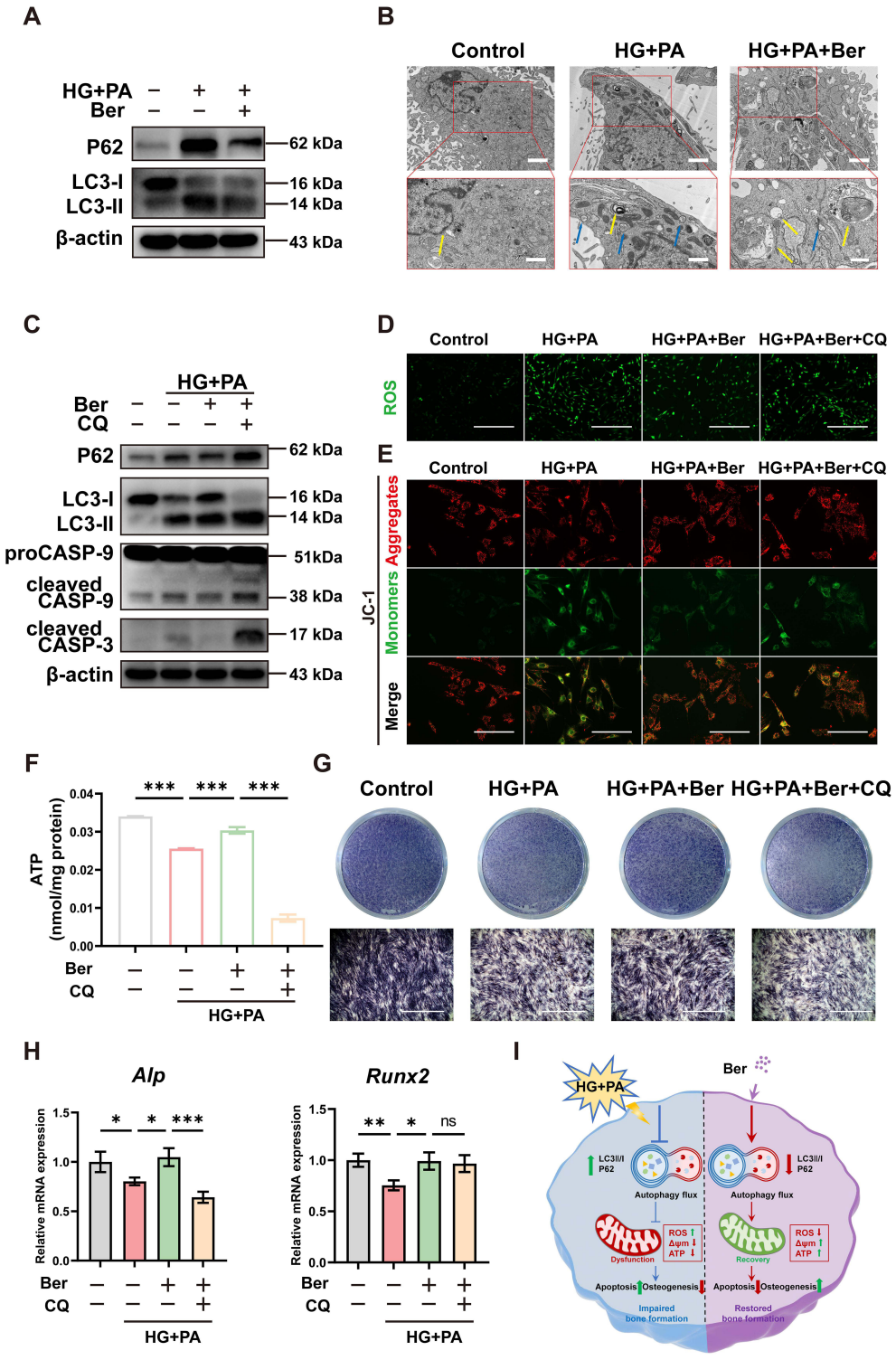

Figure 3 Berberine protected BMSCs from damage induced by HG+PA via facilitating autophagy flux. (**A**) WB assays of LC3-II/I and P62 in BMSCs from the control, HG+PA, and HG+PA+Ber groups. (**B**) Autophagosomes and autophagolysosomes in BMSCs observed by TEM after treatment in the control, HG+PA, and HG+PA+Ber groups. Blue and yellow arrowheads indicated representative autophagosomes and autolysosomes respectively. Low magnification: scale bar = 2 μm, high magnification: scale bar =1 μm. (**C**) WB assays of P62, LC3-II/I, cleaved caspase-3 and cleaved caspase-9/procaspase-9 of BMSCs in the control, HG+PA, HG+PA+Ber and HG+PA+Ber+CQ groups. Fluorescence staining of (**D**) ROS levels (scale bar: 400 μm) and (**E**) MMP (Green signal indicated monomeric JC-1, and red signal indicated aggregated JC-1. Scale bar: 200 μm) in BMSCs from the above four groups. (**F**) ATP production level and (**G**) ALP staining (scale bar: 1 mm) in BMSCs with different treatments. (**H**) qRT–PCR of the relative gene expressions of *Runx2* and *Alp* in BMSCs from different groups. (**I**) Schematic image of berberine protecting HG+PA-compromised BMSCs from damage via facilitating autophagy flux. *p < 0.05, **p < 0.01, ***p < 0.001. HG+PA, high glucose and palmitate; Ber, berberine; CQ, Chloroquine; CASP, caspase.

autophagy flux, as supported by an upregulation in the LC3-II/I and P62 level compared to HG+PA+Ber treatment (Figure 3C). Furthermore, CQ pre-treatment attenuated the therapeutic effects of berberine, as indicated by excessive ROS production (Figure 3D), MMP collapse (Figure 3E), ATP content reduction (Figure 3F), the upregulation of apoptotic-related proteins (cleaved caspase-3 and cleaved caspase-9/procaspase-9) (Figure 3C), and the downregulation of ALP staining levels and expression of osteogenic gene (Figure 3G and H). Therefore, we hypothesized that berberine could improve ROS overproduction, mitochondrial dysfunction, cellular damage and the impaired osteogenic differentiation by facilitating autophagy flux (Figure 3I). This is consistent with previous reports that berberine had exerted protective effects by promoting autophagy under different pathological conditions.[56–59] In vivo and in vitro assays indicated that berberine could enhance autophagy to reduce contrast-induced acute kidney injury.[59] He et al found that berberine were able to reduce oxidative stress damage and stabilize mitochondrial function to attenuate chronic intermittent hypoxia-induced myocardial injury through the upregulation of autophagy.[58] Nevertheless, there are also researches with the contrary conclusions. For instance, berberine was reported to inhibit excessive autophagy for protecting H9c2 cells against ischemia/reperfusion injury.[60] It may be associated with the discrepancy in cell types, and microenvironmental stimulations,[60–62] which need be further investigated.

Preparation and Characterization of Ber@SF/PCL Electrospun Membranes

Although berberine has shown potential for rescuing the impaired BMSCs induced by HG+PA, its poor solubility and bioavailability limited its application in biomedical and clinical fields. Therefore, the fabrication of a topical sustained-release delivery system is an attractive tactic for bone tissue engineering in DM. Among various local delivery systems (eg nanoparticles, micelles, liposomes, hydrogels), electrospun nanofiber is considered a favorable candidate. It can not only encapsulate drugs but also mimic the structure of bone ECM in a cost-effective and simplistic manner.[63,64] However, the unexpected burst drug release of nanofiber membranes hindered their further biomedical applications. To address this issue, core-shell nanofibers prepared using emulsion electrospinning have been used to achieve sustained and controlled drug release by embedding the drug in the core layer of the nanofiber.[65] In this study, a mixture of Ber/SF/HFIP and PCL/DCM/HFIP solution (1:1, v/v) was prepared and formed a water-in-oil emulsion through gentle stirring overnight (Figure 4A). The stability of the emulsion played a critical role in determining the core-shell structure of electrospun nanofibers (Ber@SF/PCL). TEM analysis confirmed the core-shell structure in a single nanofiber, as evident from the clear demarcation between the core and shell layers (Figure 4B), consistent with a previous literature.[38] The SEM images displayed a random distribution structure with smooth, bead-free, and homogeneous surfaces, as well as numerous pores in SF/PCL and Ber@SF/PCL nanofibers (Figure 4C), which resembled the bone ECM and could offer an advantageous microenvironment for cell adhesion and proliferation. The relative homogeneous green fluorescence observed in the laser confocal microscope (Figure 4D), confirmed the successful encapsulation and uniform distribution of berberine in the nanofibers.

Wettability, as assessed by WCA measurements, is an essential parameter for evaluating the interaction between cells and biomaterial surfaces. The SF/PCL and Ber@SF/PCL mats demonstrated high hydrophilicity with WCAs of 50.0° and 46.67°, respectively, significantly lower than the hydrophobic PCL mats (99.67°) (Figure 4E). This suggested that the incorporation of SF greatly improved the wettability of the nanofiber membranes, and the encapsulation of the hydrophobic drug berberine had little effect on their wettability. Therefore, Ber@SF/PCL membranes with good hydrophilicity are expected to enhance cell adhesion and the deposition of cellular matrix.

The chemical structure and states of the nanofibers were examined using XRD and FTIR. Firstly, we used XRD to investigate the structure of berberine, SF/PCL and Ber@SF/PCL nanofibers. In Figure 4F, sharp intense peaks at $2\theta = 10°$ to 30° were observed, indicating the presence of crystalline berberine. These peaks were not shown in the Ber@SF/PCL nanofibers, and there were only small variations in the original crystallinity between SF/PCL and Ber@SF/PCL. The above XRD results, similar to those of Ma et al,[66] suggested that berberine in the Ber@SF/PCL was prepared as an amorphous solid dispersion, which enhanced its solubility, bioavailability and stability. In Figure 4G, the spectrum of the SF/PCL nanofibers included the typical peaks of both SF and PCL, such as the peak at 2951 cm^{-1} for the C-H stretching vibration and 1728 cm^{-1} for carbonyl stretching of PCL and the amide I (1624 cm^{-1}), amide II (1518 cm^{-1}) and amide III (1256 cm^{-1}) regions of SF; and the spectrum of berberine presented peaks at 1033 cm^{-1} (C-O stretching vibration) and at 896 cm^{-1} (C-H bending vibration of the benzenoid ring). However, the spectra of Ber@SF/PCL did not differ appreciably from that of SF/PCL,

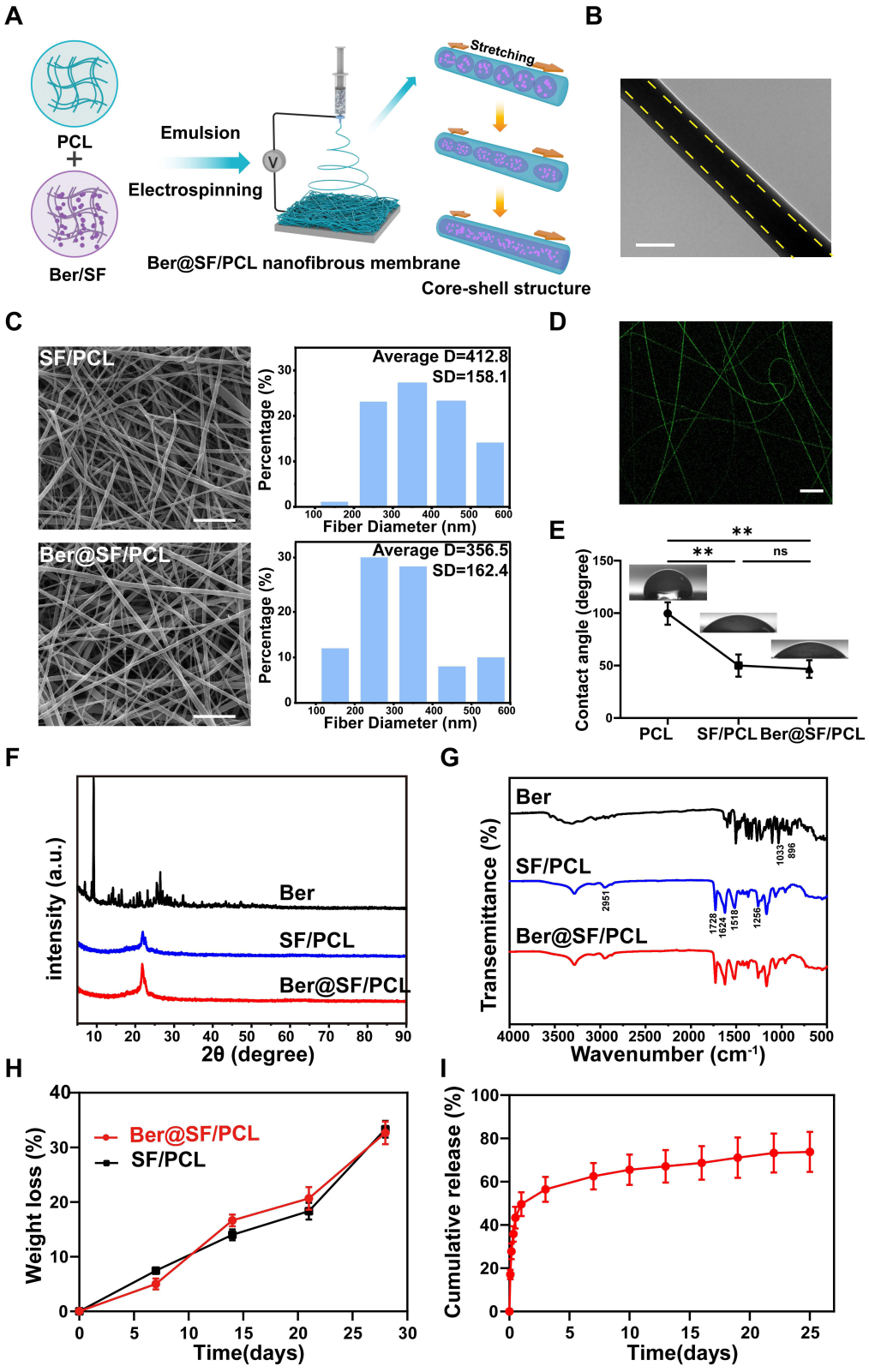

Figure 4 Construction and characterization of Ber@SF/PCL nanofiber membrane. (**A**) Schematic diagram of the fabrication of Ber@SF/PCL nanofiber membrane. (**B**) TEM photographs of Ber@SF/PCL nanofiber. The yellow dotted line indicated the clear demarcation between the core and shell layer of the single nanofiber. Scale bar: 200 nm. (**C**) SEM images of nanofiber and their average diameters of SF/PCL and Ber@SF/PCL nanofiber. Scale bar: 5 μm. (**D**) Fluorescence microscopy image of the Ber@SF/PCL nanofiber. Scale bar: 20 μm. (**E**) WCA measurements for PCL, SF/PCL and Ber@SF/PCL nanofiber. (**F**) XRD and FTIR (**G**) spectra for Berberine, SF/PCL and Ber@SF/PCL nanofiber. (**H**) Degradation rates of the SF/PCL and Ber@SF/PCL membranes incubated in PBS with protease XIV after 28 days. (**I**) In vitro release curve of berberine from Ber@SF/PCL nanofibers. **p < 0.01.

indicating no chemical interactions between berberine and the nanocarrier, and the similar results were found by Zhang et al.[67] Therefore, the drug release rate could mainly be attributed to diffusion through the polymer matrix and polymer degradation.[68] To mimic the in vivo degradation process, Ber@SF/PCL and SF/PCL membranes were co-incubated in PBS with protease XIV (300 μg/mL) at 37°C.[69] The membranes exhibited gradual degradation, as shown by increasing weight loss over time (Figure 4H). Moreover, Figure 4I depicts the cumulative release curves of berberine from Ber@SF/PCL membranes in vitro. The observed release profile showed biphasic kinetics with an initial burst-like release, followed by a sustained and stable release. In the first two hours, approximately 17.14% of berberine from Ber@SF/PCL was rapidly released, which could be attributed to the quick detachment of a few berberine distributed on the surface of the nanofibers due to the fast evaporation of the solvent during electrospinning.[43,70] This rapid release was beneficial for quickly reaching an effective drug concentration, thereby improving the abnormal diabetic microenvironment. In stage II, the remaining berberine encapsulated in the core layer of the nanofibers was slowly released in a sustained manner driven by drug diffusion through the polymer matrix. This sustained release of berberine was responsible for maintaining a local drug level over time, which was necessary for facilitating diabetic bone regeneration.

Biocompatibility Evaluations of the Ber@SF/PCL Electrospun Membranes

Biocompatibility is a critical requirement for the bone graft materials.[71] To evaluate the cytotoxicity of the membranes on BMSCs, CCK-8 assays and live/dead cell staining were performed. The relative proliferation rates in different groups were all greater than 100% on day 1 and 4 (Figure 5A). However, the 5% Ber@SF/PCL membrane showed slightly lower proliferation rate (91.9%) on day 7, compared to the other groups (Figure 5A), which could result from the increasing concentration of berberine.[27] The same trends were observed after live/dead cell staining (Figure 5B). Therefore, it was believed that both SF/PCL and Ber@SF/PCL (except 5%) nanofibers demonstrated excellent cytocompatibility. And no obvious hemolysis was observed in either of the nanofiber group after incubation with rat erythrocytes for 2 hours (Figure 5C and D), indicating good compatibility with blood. Furthermore, the in vivo bio-toxicity testing was conducted after 6 weeks of membranes implantation of the membranes. The results of H&E-stained images of internal organs in all T2DM rat groups showed no appreciable inflammatory response or organ damage (Figure 5E), thus further confirming the biocompatibility of Ber@SF/PCL nanofibers.

Ber@SF/PCL Electrospun Membranes Promoted Alveolar Bone Regeneration in T2DM Rats

The in vitro investigation on the actions of berberine indicated that it could ameliorate ROS overproduction, mitochondrial dysfunction, cell apoptosis and improve osteogenesis differentiation under HG+PA conditions. To efficiently deliver berberine to the alveolar bone defect area in T2DM rats, we successfully constructed a topical sustained-release nano-delivery system (Ber@SF/PCL). This system demonstrated excellent physicochemical properties and good cytocompatibility. Therefore, we investigated its ability to promote alveolar bone repair in T2DM rats. The schematic procedure of the in vivo experiment is depicted in Figure 6A. Firstly, we established T2DM rat models by feeding rats a high-fat diet for 4 weeks, followed by intraperitoneal administration of STZ. After 7 and 14 days, the random blood glucose levels (Figure S1) of the rats were more than 16.7 mmol/L in T2DM model groups accompanied by polydipsia, polyphagia, polyuria, and emaciation, which suggested that the T2DM rat model was successfully constructed. The rat alveolar bone fenestration model, which involves a regular burr hole defect in the periapical region of the mandibular posterior teeth, has been widely used to evaluate the ability of different biomaterials in alveolar bone remodelling.[46,72–74] Therefore, we created a standard round bone defect (3 mm in diameter and 1 mm in depth) in the periapical region between the first and second molars based on previous reports with minor alterations (Figure S2).[72,75] To assess whether the Ber@SF/PCL electrospun nanofibrous membranes could enhance diabetic bone regeneration, the nanofibers were implanted into the alveolar bone defects.

Figure 6B shows the 3D reconstructed and cross-section images produced by μ-CT scanning of rat alveolar bone defects which are marked in yellow at 2 and 6 weeks postoperatively. The results suggested that alveolar bone healing was significantly delayed in the T2DM group at 2 weeks, with minimal formation of new bone at the defect margin,

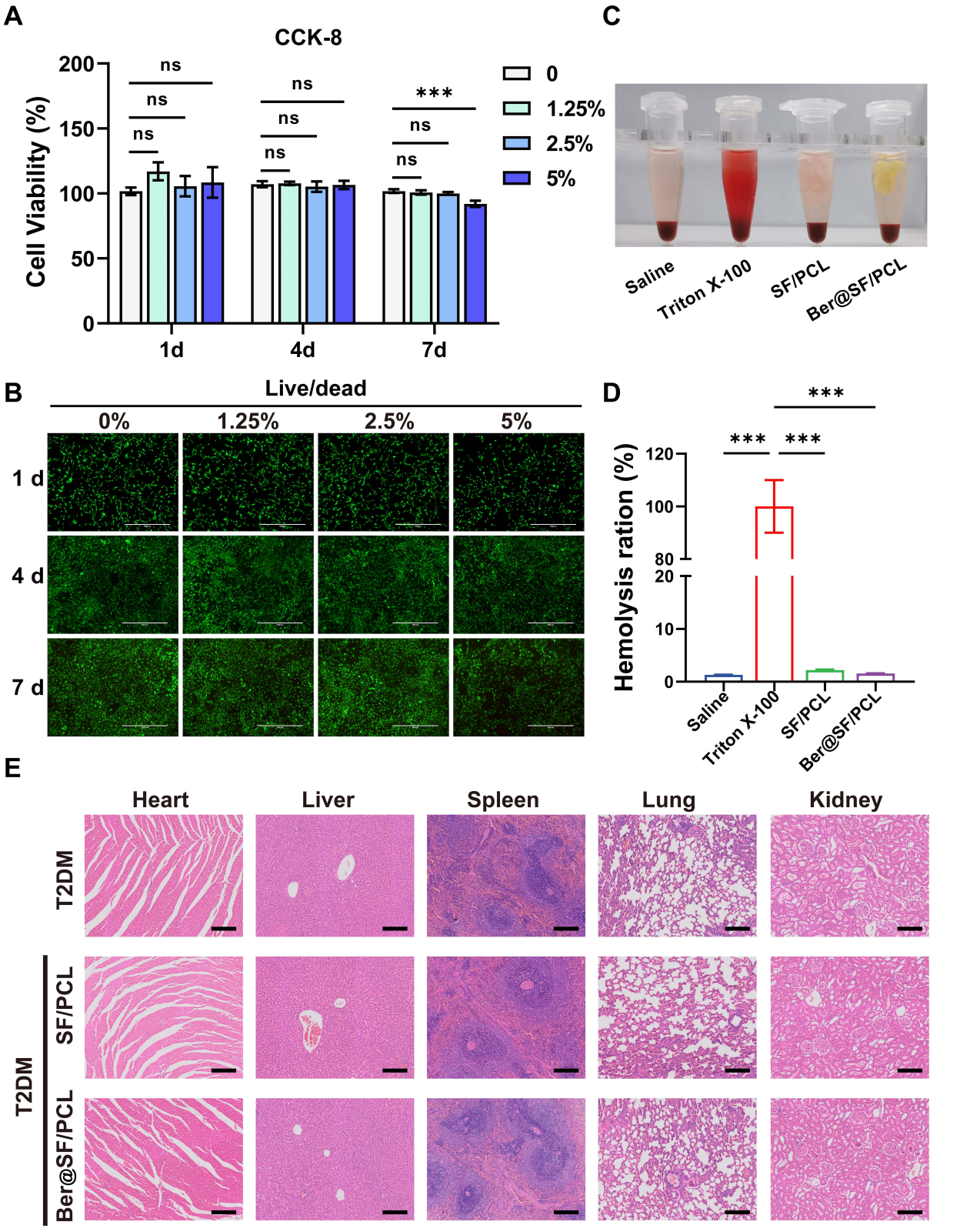

Figure 5 Biocompatibility of Ber@SF/PCL nanofiber membrane. (**A**) Proliferation ability of BMSCs treated with the condition medium (0%, 1.25%, 2.5%, 5%) for 1, 4, 7 days. (**B**) Live/dead cell staining of Ber@SF/PCL nanofiber membranes with different concentrations of berberine. Green signals indicated live cells, and red signals indicated dead cells. Scale bar: 1000 μm. (**C**) The hemolysis situations of SF/PCL and Ber@SF/PCL nanofiber membranes coincubated with rat red blood cells for two hours and (**D**) their quantitative analysis. (**E**) H&E staining of heart, liver, spleen, lung, kidney tissues of T2DM rats implanted with the nanofibers at 6 weeks postoperatively. Scale bar: 200 μm. ***$p < 0.001$.

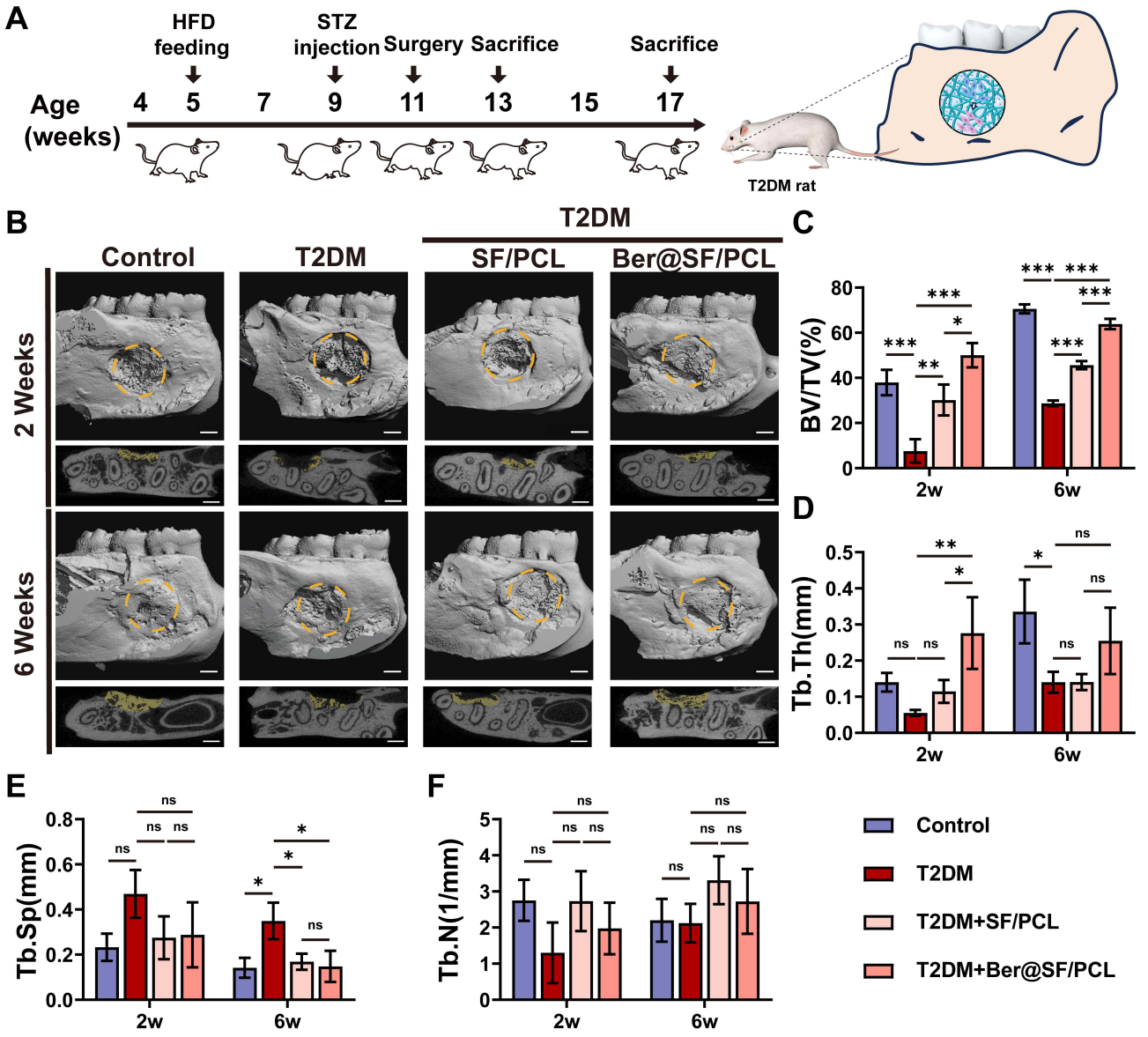

Figure 6 Ber@SF/PCL nanofiber membranes improved alveolar bone regeneration in T2DM rats. (**A**) In vivo experiment schematic procedure. (**B**) 3D reconstructed and cross-section images of rat alveolar bone defects. Yellow dotted circle indicated the region of interest for μ-CT analysis. The new bone in the defect region was labelled in yellow. Scale bar: 1 mm. Quantification of (**C**) BV/TV, (**D**) Tb.Th, (**E**) Tb.Sp, and (**F**) Tb.N. *p < 0.05, **p < 0.01, ***p < 0.001.

which corresponded to the impaired osteogenic capacity of BMSCs in the HG+PA environment observed from in vitro assays. However, the T2DM+Ber@SF/PCL group displayed the most regenerated bone formation compared to the other T2DM groups at 2 or 6 weeks. The findings were similar to the quantification of BV/TV in all groups (Figure 6C). Furthermore, bone microarchitecture was closely associated with the quality of nascent bone.[76] Tb.Th of the T2DM +Ber@SF/PCL group was greater than that of the other T2DM groups at 2 weeks (Figure 6D), and Tb.Sp of the T2DM +Ber@SF/PCL group was less than that of the T2DM group at 6 weeks (Figure 6E). However, Tb.N did not significantly differ among groups (Figure 6F), which was similar to the results of previous studies and might be associated with osteoporotic bone defects in DM.[73,77] Taken together, berberine could improve alveolar bone regeneration in T2DM rats, which were consistent with the protective effects of berberine observed in in vitro assays with HG+PA-compromised BMSCs.

Histological analyses were conducted using H&E, Masson's trichrome and immunohistochemical staining (Figure 7A–C) to further evaluate the newly formed tissues at the defect sites. At 2 weeks, the alveolar bone defect

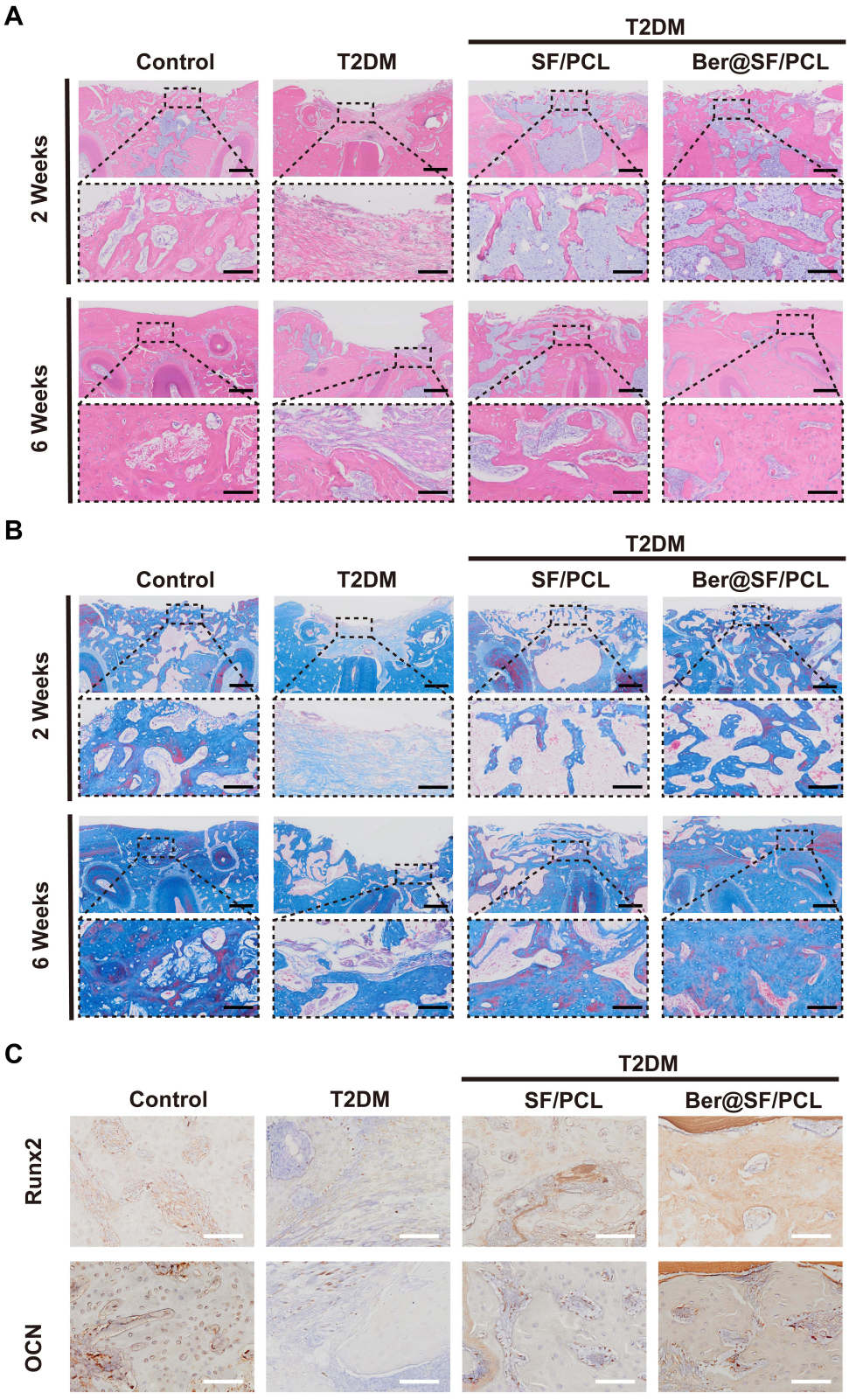

Figure 7 Histological evaluation of alveolar bone defects. H&E (**A**) and Masson (**B**) staining images of the bone defect. Low magnification: scale bar = 400 μm, high magnification: scale bar = 100 μm. (**C**) Immunohistochemical staining of the osteogenic marker Runx2 after 2 weeks and OCN after 6 weeks. Scale bar =100 μm.

area of T2DM group was filled with plenty of fibrous tissues, with minimal osteoid bone tissues around the margin. In contrast, the T2DM+SF/PCL and T2DM+Ber@SF/PCL group showed varying amounts of newly formed bone and bone marrow with no evident inflammatory cells. It might be due to the fact that electrospun nanofibrous membranes acted as a barrier to prevent the invasion of epithelium from the adjacent connective tissues and created a sufficient and favorable space for bone healing. Notably, the T2DM+Ber@SF/PCL group exhibited more spongy bone formation, indicated by blue-stained collagen type I compared to the T2DM+SF/PCL group, suggesting robust bone regeneration. After 6 weeks, there were still some fibrous tissues appearing in the incompletely closed bone defect in the T2DM group, although more new bone had formed compared to the 2-week mark. Moreover, in contrast to the T2DM+SF/PCL group, the T2DM +Ber@SF/PCL group exhibited more active bone remodeling, with spongy bone being replaced by more mature woven bone containing increasing amounts of bone collagen fibers. Lastly, Figure 7C shows the immunohistochemical staining of Runx2 and OCN. Runx2, a marker of bone formation and remodeling during the early stage of osteoblast differentiation,[78] was more highly expressed in the T2DM+Ber@SF/PCL group at 2 weeks compared to the other groups. OCN, a specific marker for late osteoblast differentiation and mineralization stage,[79] exhibited a consistent trend with Runx2 expression at 6 weeks among all groups. Several previous studies also demonstrated that local delivery of berberine via the biomaterials had the ability to increase the expression of osteogenic proteins and regenerate bone.[67,80,81] Recently, increasing evidence demonstrated that diabetes-mediated oxidative stress and mitochondrial dysfunction involve in the failure of alveolar bone regeneration.[10,48] Hu et al proved that reversing mitochondrial dysfunction could improve the osteointegration of titanium implant in DM.[82] Wang et al also reported that the release of metformin could reduce the overproduced ROS to restore osteogenesis in the HG environment.[46] Therefore, we assumed the potential mechanisms by which the Ber@SF/PCL electrospun membranes promoted diabetic alveolar bone healing. Firstly, it is crucial to be noted that the topical delivery and sustained release of berberine from Ber@SF/PCL electrospun membranes could scavenge ROS and improve mitochondrial dysfunction to improve adverse diabetic microenvironment, thus promoting alveolar bone regeneration. Next, Ber@SF/PCL electrospun membranes, which had excellent physico-chemical properties and good cytocompatibility, also offer an advantageous space for new bone formation.

To our knowledge, multiple bioactive materials have been developed to promote bone regeneration. However, some of these researches paid no attention to the regulation of the specific microenvironment under the pathological condition and the exploration of potential therapeutic mechanism, thus limiting their clinical application.[64,66,83] In this study, we firstly found berberine can improve the adverse diabetic osteogenic microenvironment through ameliorating oxidative damage and mitochondrial dysfunction via the restoration of autophagy flux. Moreover, to improve the bioavailability of berberine, we constructed a novel berberine-loaded nanocarrier (Ber@SF/PCL) using the emulsion electrospinning to safely and effectively regulate the pathological microenvironment and simultaneously promote alveolar bone regeneration in T2DM rats. Therefore, this novel composite electrospun nanofibrous membrane shows promise as a precise and cost-effectiveness biomaterial for use in alveolar bone tissue engineering for DM. Additionally, this therapeutic strategy might be expanded to the delivery of other osteo-inductive drug or bioactive molecule with low bioavailability. In the future, we intend to further explore the other underlying therapeutic mechanism and investigate the pharmacodynamics of this nanomaterial, particularly, its distribution, absorption, and metabolism in vivo so as to better optimize our nano-delivery system.

Conclusion

Our study showed berberine could inhibit ROS overproduction, mitochondrial dysfunction, cell apoptosis and improved osteogenesis differentiation by restoring autophagy flux under HG+PA conditions to a certain extent. To improve the bioavailability of berberine, we constructed a novel berberine-loaded nanocarrier (Ber@SF/PCL) using the emulsion electrospinning. In vitro studies demonstrated excellent physicochemical properties and good cytocompatibility of the Ber@SF/PCL electrospun nanomembranes. Furthermore, the alveolar bone remodeling in a T2DM rat was significantly improved with Ber@SF/PCL. Therefore, our work addresses the fundamental problem of how berberine rescues HG+PA-compromised BMSCs and provides a new research idea for alveolar bone tissue engineering under diabetic conditions.

Acknowledgments

This work was supported by the National Natural Science Foundation of China (No. 82471016, No. 81470772), the Program for Youth Innovation in Future Medicine, Chongqing Medical University (W0033), Chongqing Medical Scientific Research Project (cstc2020jcyj-msxmX0307, CSTB2023NSCQ-MSX0233), and Chongqing Talent Program: Innovative leading talents (Medical field, CQYC20210303384).

Disclosure

The authors report no conflicts of interest in this work.

References

1. Shanbhag S, Pandis N, Mustafa K, Nyengaard JR, Stavropoulos A. Alveolar bone tissue engineering in critical-size defects of experimental animal models: A systematic review and meta-analysis. *J Tissue Eng Regen Med*. 2017;11(10):2935–2949. doi:10.1002/term.2198
2. Kassebaum NJ, Bernabé E, Dahiya M, Bhandari B, Murray CJ, Marcenes W. Global burden of severe periodontitis in 1990-2010: A systematic review and meta-regression. *J Dent Res*. 2014;93(11):1045–1053. doi:10.1177/0022034514552491
3. Wu CZ, Yuan YH, Liu HH, et al. Epidemiologic relationship between periodontitis and type 2 diabetes mellitus. *BMC Oral Health*. 2020;20(1):204. doi:10.1186/s12903-020-01180-w
4. Lecka-Czernik B. Diabetes, bone and glucose-lowering agents: Basic biology. *Diabetol*. 2017;60(7):1163–1169. doi:10.1007/s00125-017-4269-4
5. Hajishengallis G, Chavakis T. Local and systemic mechanisms linking periodontal disease and inflammatory comorbidities. *Nat Rev Immunol*. 2021;21(7):426–440. doi:10.1038/s41577-020-00488-6
6. Compston J. Type 2 diabetes mellitus and bone. *J Intern Med*. 2018;283(2):140–153. doi:10.1111/joim.12725
7. Graves DT, Ding Z, Yang Y. The impact of diabetes on periodontal diseases. *Periodontol 2000*. 2020;82(1):214–224. doi:10.1111/prd.12318
8. Global. regional, and national burden of diabetes from 1990 to 2021, with projections of prevalence to 2050: A systematic analysis for the global burden of disease study 2021. *Lancet*. 2023;402(10397):203–234. doi:10.1016/s0140-6736(23)01301-6.
9. Jiao H, Xiao E, Graves DT. Diabetes and its effect on bone and fracture healing. *Curr Osteoporos Rep*. 2015;13(5):327–335. doi:10.1007/s11914-015-0286-8
10. Wang X, Wang H, Zhang T, Cai L, Kong C, He J. Current knowledge regarding the interaction between oral bone metabolic disorders and diabetes mellitus. *Front Endocrinol*. 2020;11:536. doi:10.3389/fendo.2020.00536
11. Zhang Q, Zhang X, Yang B, et al. Ligustilide-loaded liposome ameliorates mitochondrial impairments and improves cognitive function via the PKA/AKAP1 signaling pathway in a mouse model of alzheimer's disease. *CNS Neurosci Ther*. 2023;30(3):e14460. doi:10.1111/cns.14460
12. Willems PH, Rossignol R, Dieteren CE, Murphy MP, Koopman WJ. Redox homeostasis and mitochondrial dynamics. *Cell Metab*. 2015;22(2):207–218. doi:10.1016/j.cmet.2015.06.006
13. Gan X, Huang S, Liu Y, Yan SS, Yu H. The potential role of damage-associated molecular patterns derived from mitochondria in osteocyte apoptosis and bone remodeling. *Bone*. 2014;62:67–68. doi:10.1016/j.bone.2014.01.018
14. Tao H, Zhu P, Xia W, et al. The emerging role of the mitochondrial respiratory chain in skeletal aging. *Aging Dis*. 2023;15(4):1784. doi:10.14336/ad.2023.0924
15. Prentki M, Corkey BE. Are the beta-cell signaling molecules malonyl-CoA and cystolic long-chain acyl-CoA implicated in multiple tissue defects of obesity and NIDDM? *Diabetes*. 1996;45(3):273–283. doi:10.2337/diab.45.3.273
16. Lytrivi M, Castell AL, Poitout V, Cnop M. Recent insights into mechanisms of β-cell lipo- and glucolipotoxicity in type 2 diabetes. *J Mol Biol*. 2020;432(5):1514–1534. doi:10.1016/j.jmb.2019.09.016
17. Dikic I, Elazar Z. Mechanism and medical implications of mammalian autophagy. *Nat Rev Mol Cell Biol*. 2018;19(6):349–364. doi:10.1038/s41580-018-0003-4
18. Nixon RA. The role of autophagy in neurodegenerative disease. *Nat Med*. 2013;19(8):983–997. doi:10.1038/nm.3232
19. Feng X, Sureda A, Jafari S, et al. Berberine in cardiovascular and metabolic diseases: From mechanisms to therapeutics. *Theranostics*. 2019;9(7):1923–1951. doi:10.7150/thno.30787
20. Gao Y, Wang F, Song Y, Liu H. The status of and trends in the pharmacology of berberine: A bibliometric review [1985-2018]. *Chin Med*. 2020;15:7. doi:10.1186/s13020-020-0288-z
21. Xu D, Yang W, Zhou C, Liu Y, Xu B. Preventive effects of berberine on glucocorticoid-induced osteoporosis in rats. *Planta Med*. 2010;76(16):1809–1813. doi:10.1055/s-0030-1250040
22. Tao K, Xiao D, Weng J, Xiong A, Kang B, Zeng H. Berberine promotes bone marrow-derived mesenchymal stem cells osteogenic differentiation via canonical Wnt/β-catenin signaling pathway. *Toxicol Lett*. 2016;240(1):68–80. doi:10.1016/j.toxlet.2015.10.007
23. Liu J, Zhao X, Pei D, et al. The promotion function of Berberine for osteogenic differentiation of human periodontal ligament stem cells via ERK-FOS pathway mediated by EGFR. *Sci Rep*. 2018;8(1):2848. doi:10.1038/s41598-018-21116-3
24. Qin X, Zhao Y, Gong J, et al. Berberine protects glomerular podocytes via inhibiting Drp1-mediated mitochondrial fission and dysfunction. *Theranostics*. 2019;9(6):1698–1713. doi:10.7150/thno.30640
25. Wang Y, Liao J, Luo Y, et al. Berberine alleviates doxorubicin-induced myocardial injury and fibrosis by eliminating oxidative stress and mitochondrial damage via promoting Nrf-2 pathway activation. *Int J Mol Sci*. 2023;24(4):3257. doi:10.3390/ijms24043257
26. Li S, Jiang Y, Xing X, et al. Protective mechanism of berberine on human retinal pigment epithelial cells against apoptosis induced by hydrogen peroxide via the stimulation of autophagy. *Oxid Med Cell Longev*. 2021;2021:7654143. doi:10.1155/2021/7654143
27. Chen B, Zhang JP. Bcl-xL is required for the protective effects of low-dose berberine against doxorubicin-induced cardiotoxicity through blocking apoptosis and activating mitophagy-mediated ROS elimination. *Phytomed*. 2022;101:154130. doi:10.1016/j.phymed.2022.154130
28. Ye K, Kuang H, You Z, Morsi Y, Mo X. Electrospun nanofibers for tissue engineering with drug loading and release. *Pharmaceutics*. 2019;11(4). doi:10.3390/pharmaceutics11040182

29. Lan X, Wang H, Bai J, et al. Multidrug-loaded electrospun micro/nanofibrous membranes: Fabrication strategies, release behaviors and applications in regenerative medicine. *J Cont Rel*. 2021;330:1264–1287. doi:10.1016/j.jconrel.2020.11.036
30. Wang Z, Wang Y, Yan J, et al. Pharmaceutical electrospinning and 3D printing scaffold design for bone regeneration. *Adv Drug Deliv Rev*. 2021;174:504–534. doi:10.1016/j.addr.2021.05.007
31. Anjum S, Rahman F, Pandey P, et al. Electrospun biomimetic nanofibrous scaffolds: A promising prospect for bone tissue engineering and regenerative medicine. *Int J Mol Sci*. 2022;23(16):9206. doi:10.3390/ijms23169206
32. Zhang X, Tsukada M, Morikawa H, Aojima K, Zhang G, Miura M. Production of silk sericin/silk fibroin blend nanofibers. *Nanoscale Res Lett*. 2011;6:510. doi:10.1186/1556-276x-6-510
33. Huang W, Ling S, Li C, Omenetto FG, Kaplan DL. Silkworm silk-based materials and devices generated using bio-nanotechnology. *Chem Soc Rev*. 2018;47(17):6486–6504. doi:10.1039/c8cs00187a
34. Wei S, Ma JX, Xu L, Gu XS, Ma XL. Biodegradable materials for bone defect repair. *Mil Med Res*. 2020;7(1):54. doi:10.1186/s40779-020-00280-6
35. Agarwal Y, Rajinikanth PS, Ranjan S, et al. Curcumin loaded polycaprolactone-/polyvinyl alcohol-silk fibroin based electrospun nanofibrous mat for rapid healing of diabetic wound: An in-vitro and in-vivo studies. *Int J Biol Macromol*. 2021;176:376–386. doi:10.1016/j.ijbiomac.2021.02.025
36. Abadi B, Goshtasbi N, Bolourian S, Tahsili J, Adeli-Sardou M, Forootanfar H. Electrospun hybrid nanofibers: Fabrication, characterization, and biomedical applications. *Front Bioeng Biotechnol*. 2022;10:986975. doi:10.3389/fbioe.2022.986975
37. Guo B, Ma PX. Conducting polymers for tissue engineering. *Biomacromol*. 2018;19(6):1764–1782. doi:10.1021/acs.biomac.8b00276
38. Wang Z, Song X, Cui Y, et al. Silk fibroin H-fibroin/poly(ε-caprolactone) core-shell nanofibers with enhanced mechanical property and long-term drug release. *J Colloid Interface Sci*. 2021;593:142–151. doi:10.1016/j.jcis.2021.02.099
39. Chen Y, Hu Y, Yang L, et al. Runx2 alleviates high glucose-suppressed osteogenic differentiation via PI3K/AKT/GSK3β/β-catenin pathway. *Cell Biol Int*. 2017;41(8):822–832. doi:10.1002/cbin.10779
40. Ma H, Wang X, Zhang W, et al. Melatonin suppresses ferroptosis induced by high glucose via activation of the Nrf2/HO-1 signaling pathway in type 2 diabetic osteoporosis. *Oxid Med Cell Longev*. 2020;2020:9067610. doi:10.1155/2020/9067610
41. Ai D, Yin Y, Xia X, et al. Validation of a physiological type 2 diabetes model in human periodontal ligament stem cells. *Oral Dis*. 2023;30 (5):3363–3375. doi:10.1111/odi.14766
42. Xiang J, Li Y, Ren M, et al. Sandwich-like nanocomposite electrospun silk fibroin membrane to promote osteogenesis and antibacterial activities. *Appl Mater Today*. 2022;26:101273. doi:10.1016/j.apmt.2021.101273
43. Li L, Li H, Qian Y, et al. Electrospun poly (ε-caprolactone)/silk fibroin core-sheath nanofibers and their potential applications in tissue engineering and drug release. *Int J Biol Macromol*. 2011;49(2):223–232. doi:10.1016/j.ijbiomac.2011.04.018
44. Srinivasan K, Viswanad B, Asrat L, Kaul CL, Ramarao P. Combination of high-fat diet-fed and low-dose streptozotocin-treated rat: a model for type 2 diabetes and pharmacological screening. *Pharmacol Res*. 2005;52(4):313–320. doi:10.1016/j.phrs.2005.05.004
45. Kleinert M, Clemmensen C, Hofmann SM, et al. Animal models of obesity and diabetes mellitus. *Nat Rev Endocrinol*. 2018;14(3):140–162. doi:10.1038/nrendo.2017.161
46. Wang H, Chang X, Ma Q, et al. Bioinspired drug-delivery system emulating the natural bone healing cascade for diabetic periodontal bone regeneration. *Bioact Mater*. 2023;21:324–339. doi:10.1016/j.bioactmat.2022.08.029
47. Wang J, Liu S, Li J, Zhao S, Yi Z. Roles for miRNAs in osteogenic differentiation of bone marrow mesenchymal stem cells. *Stem Cell Res Ther*. 2019;10(1):197. doi:10.1186/s13287-019-1309-7
48. Tanios M, Brickman B, Cage E, et al. Diabetes and impaired fracture healing: A narrative review of recent literature. *Curr Osteoporos Rep*. 2022;20 (5):229–239. doi:10.1007/s11914-022-00740-z
49. Xu X, Wang X, Yang Y, et al. Neonicotinoids: mechanisms of systemic toxicity based on oxidative stress-mitochondrial damage. *Arch Toxicol*. 2022;96(6):1493–1520. doi:10.1007/s00204-022-03267-5
50. Gao J, Feng Z, Wang X, et al. SIRT3/SOD2 maintains osteoblast differentiation and bone formation by regulating mitochondrial stress. *Cell Death Differ*. 2018;25(2):229–240. doi:10.1038/cdd.2017.144
51. Zhang LN, Wang XX, Wang Z, Li KY, Xu BH, Zhang J. Berberine improves advanced glycation end products-induced osteogenic differentiation responses in human periodontal ligament stem cells through the canonical Wnt/β-catenin pathway. *Mol Med Rep*. 2019;19(6):5440–5452. doi:10.3892/mmr.2019.10193
52. Shao J, Liu S, Zheng X, Chen J, Li L, Zhu Z. Berberine promotes peri-implant osteogenesis in diabetic rats by ROS-mediated IRS-1 pathway. *Biofactors*. 2021;47(1):80–92. doi:10.1002/biof.1692
53. Kim KH, Lee MS. Autophagy–a key player in cellular and body metabolism. *Nat Rev Endocrinol*. 2014;10(6):322–337. doi:10.1038/nrendo.2014.35
54. Zhu C, Shen S, Zhang S, Huang M, Zhang L, Chen X. Autophagy in bone remodeling: A regulator of oxidative stress. *Front Endocrinol*. 2022;13:898634. doi:10.3389/fendo.2022.898634
55. Gump JM, Thorburn A. Autophagy and apoptosis: What is the connection? *Trends Cell Biol*. 2011;21(7):387–392. doi:10.1016/j.tcb.2011.03.007
56. Jin Y, Liu S, Ma Q, Xiao D, Chen L. Berberine enhances the AMPK activation and autophagy and mitigates high glucose-induced apoptosis of mouse podocytes. *Eur J Pharmacol*. 2017;794:106–114. doi:10.1016/j.ejphar.2016.11.037
57. Luo R, Liao Z, Song Y, et al. Berberine ameliorates oxidative stress-induced apoptosis by modulating ER stress and autophagy in human nucleus pulposus cells. *Life Sci*. 2019;228:85–97. doi:10.1016/j.lfs.2019.04.064
58. Zhou Z, Zhao Q, Huang Y, et al. Berberine ameliorates chronic intermittent hypoxia-induced cardiac remodelling by preserving mitochondrial function, role of SIRT6 signalling. *J Cell Mol Med*. 2024;28(12):e18407. doi:10.1111/jcmm.18407
59. Zuo Z, Li Q, Zhou S, et al. Berberine ameliorates contrast-induced acute kidney injury by regulating HDAC4-FoxO3a axis-induced autophagy: In vivo and in vitro. *Phytother Res*. 2024;38(4):1761–1780. doi:10.1002/ptr.8059
60. Hu F, Hu T, Qiao Y, et al. Berberine inhibits excessive autophagy and protects myocardium against ischemia/reperfusion injury via the RhoE/AMPK pathway. *Int J Mol Med*. 2024;53(5). doi:10.3892/ijmm.2024.5373
61. Gruber HE, Hoelscher GL, Ingram JA, Bethea S, Hanley EN. Autophagy in the degenerating human intervertebral disc: In vivo molecular and morphological evidence, and induction of autophagy in cultured annulus cells exposed to proinflammatory cytokines-implications for disc degeneration. *Spine*. 2015;40(11):773–782. doi:10.1097/brs.0000000000000865

62. Zhang SJ, Yang W, Wang C, et al. Autophagy: A double-edged sword in intervertebral disk degeneration. *Clin Chim Acta*. 2016;457:27–35. doi:10.1016/j.cca.2016.03.016
63. Etter EL, Mei KC, Nguyen J. Delivering more for less: Nanosized, minimal-carrier and pharmacoactive drug delivery systems. *Adv Drug Deliv Rev*. 2021;179:113994. doi:10.1016/j.addr.2021.113994
64. Wu M, Han Z, Liu W, et al. Silk-based hybrid microfibrous mats as guided bone regeneration membranes. *J Mater Chem B*. 2021;9(8):2025–2032. doi:10.1039/d0tb02687e
65. Roy T, Maity PP, Rameshbabu AP, et al. Core-shell nanofibrous scaffold based on polycaprolactone-silk fibroin emulsion electrospinning for tissue engineering applications. *Bioeng*. 2018;5(3):68. doi:10.3390/bioengineering5030068
66. Ma L, Yu Y, Liu H, et al. Berberine-releasing electrospun scaffold induces osteogenic differentiation of DPSCs and accelerates bone repair. *Sci Rep*. 2021;11(1):1027. doi:10.1038/s41598-020-79734-9
67. Zhang Y, Wang T, Li J, et al. Bilayer membrane composed of mineralized collagen and chitosan cast film coated with berberine-loaded PCL/PVP electrospun nanofiber promotes bone regeneration. *Orig Res Front Bioeng Biotechnol*. 2021;9:684335. doi:10.3389/fbioe.2021.684335
68. Puppi D, Piras AM, Detta N, Dinucci D, Chiellini F. Poly(lactic-co-glycolic acid) electrospun fibrous meshes for the controlled release of retinoic acid. *Acta Biomater*. 2010;6(4):1258–1268. doi:10.1016/j.actbio.2009.08.015
69. Numata K, Cebe P, Kaplan DL. Mechanism of enzymatic degradation of beta-sheet crystals. *Biomat*. 2010;31(10):2926–2933. doi:10.1016/j.biomaterials.2009.12.026
70. Janjic M, Pappa F, Karagkiozaki V, Gitas C, Ktenidis K, Logothetidis S. Surface modification of endovascular stents with rosuvastatin and heparin-loaded biodegradable nanofibers by electrospinning. *Int J Nanomed*. 2017;12:6343–6355. doi:10.2147/ijn.s138261
71. Zeimaran E, Pourshahrestani S, Fathi A, et al. Advances in bioactive glass-containing injectable hydrogel biomaterials for tissue regeneration. *Acta Biomater*. 2021;136:1–36. doi:10.1016/j.actbio.2021.09.034
72. Padial-Molina M, Rodriguez JC, Volk SL, Rios HF. Standardized in vivo model for studying novel regenerative approaches for multitissue bone-ligament interfaces. *Nat Protoc*. 2015;10(7):1038–1049. doi:10.1038/nprot.2015.063
73. Jing X, Wang S, Tang H, et al. Dynamically bioresponsive DNA hydrogel incorporated with dual-functional stem cells from apical papilla-derived exosomes promotes diabetic bone regeneration. *ACS Appl Mater Interfaces*. 2022;14(14):16082–16099. doi:10.1021/acsami.2c02278
74. Liu S, Wang W, Wu P, et al. Pathogenesis-guided engineering of multi-bioactive hydrogel co-delivering inflammation-resolving nanotherapy and pro-osteogenic protein for bone regeneration. *Adv Funct Mater*. 2023;33(32):2301523. doi:10.1002/adfm.202301523
75. Hu Z, Ma C, Rong X, Zou S, Liu X. Immunomodulatory ECM-like microspheres for accelerated bone regeneration in diabetes mellitus. *ACS Appl Mater Interfaces*. 2018;10(3):2377–2390. doi:10.1021/acsami.7b18458
76. Lin Z, Wu J, Qiao W, et al. Precisely controlled delivery of magnesium ions thru sponge-like monodisperse PLGA/nano-MgO-alginate core-shell microsphere device to enable in-situ bone regeneration. *Biomat*. 2018;174:1–16. doi:10.1016/j.biomaterials.2018.05.011
77. Gao X, Al-Baadani MA, Wu M, et al. Study on the local anti-osteoporosis effect of polaprezinc-loaded antioxidant electrospun membrane. *Int J Nanomed*. 2022;17:17–29. doi:10.2147/ijn.s341216
78. Tang Q, Li X, Lai C, et al. Fabrication of a hydroxyapatite-PDMS microfluidic chip for bone-related cell culture and drug screening. *Bioact Mater*. 2021;6(1):169–178. doi:10.1016/j.bioactmat.2020.07.016
79. Ma Q, Jiang N, Liang S, et al. Functionalization of a clustered TiO2 nanotubular surface with platelet derived growth factor-BB covalent modification enhances osteogenic differentiation of bone marrow mesenchymal stem cells. *Biomat*. 2020;230:119650. doi:10.1016/j.biomaterials.2019.119650
80. Huang D, Zuo Y, Zou Q, et al. Antibacterial chitosan coating on nano-hydroxyapatite/polyamide66 porous bone scaffold for drug delivery. *J Biomater Sci Polym Ed*. 2011;22(7):931–944. doi:10.1163/092050610x496576
81. Chen P, Xia C, Mo J, Mei S, Lin X, Fan S. Interpenetrating polymer network scaffold of sodium hyaluronate and sodium alginate combined with berberine for osteochondral defect regeneration. *Mater Sci Eng C Mater Biol Appl*. 2018;91:190–200. doi:10.1016/j.msec.2018.05.034
82. Hu XF, Wang L, Lu YZ, et al. Adiponectin improves the osteointegration of titanium implant under diabetic conditions by reversing mitochondrial dysfunction via the AMPK pathway in vivo and in vitro. *Acta Biomater*. 2017;61:233–248. doi:10.1016/j.actbio.2017.06.020
83. Meng D, Song J, Yi Y, et al. Controlled released naringin-loaded liposome/sucrose acetate isobutyrate hybrid depot for osteogenesis in vitro and in vivo. *Front Bioeng Biotechnol*. 2022;10:1097178. doi:10.3389/fbioe.2022.1097178